Tahmasbi, A., Ward, E. S., and Ober, R. J. New results on the single molecule localization problem in two and three dimensions. Proceedings of the SPIE, Nanoimaging and Nanospectroscopy III, 9554: 955402, Aug. 2015, San Diego, CA

doi: 10.1117/12.2192008

keywords: {Cramér-Rao lower bound, Fisher information matrix, Single molecule microscopy, splines},

URL: http://proceedings.spiedigitallibrary.org/proceeding.aspx?articleid=2432531

Invited Paper

New results on the single molecule localization problem in two and three dimensions

Amir Tahmasbi[a,b], E. Sally Ward[b,d], and Raimund J. Ober[a,b]

[a]Department of Biomedical Engineering, Texas A&M University, College Station, TX, USA;
[b]Department of Molecular and Cellular Medicine, Texas A&M Health Science Center, College Station, TX, USA;
[d]Department of Microbial Pathogenesis and Immunology, Texas A&M Health Science Center, College Station, TX, USA

ABSTRACT

Fluorescence microscopy is an optical microscopy technique which has been extensively used to study specifically-labeled subcellular objects, such as proteins, and their functions. The best possible accuracy with which an object of interest can be localized when imaged using a fluorescence microscope is typically calculated using the Cramér-Rao lower bound (CRLB). The calculation of the CRLB, however, so far relied on an analytical expression for the image of the object. This can pose challenges in practice since it is often difficult to find appropriate analytical models for the images of general objects. Even if an appropriate analytical model is available, the lack of knowledge about the precise values of imaging parameters might also impose difficulties in the calculation of the CRLB. To address these challenges, we have developed an approach that directly uses an experimentally collected image set to calculate the best possible localization accuracy for a general subcellular object in two and three dimensions. In this approach, we fit smoothly connected piecewise polynomials, known as splines, to the experimentally collected image set to provide a continuous model of the object. This continuous model can then be used for the calculation of the best possible localization accuracy.

Keywords: Cramér-Rao lower bound, Fisher information matrix, single molecule microscopy, splines

1. INTRODUCTION

Fluorescence microscopy is a photon-limited imaging modality that allows the study of subcellular objects, such as single molecules, and processes with high specificity.[1–3] A central question in fluorescence microscopy concerns the best possible accuracy, in terms of standard deviation, with which an object of interest can be localized.[4] This is of significant importance in localization-based superresolution microscopy where the spatial resolution is tied to the localization accuracy.[1,5] The best possible accuracy with which an object of interest can be localized when imaged using a fluorescence microscope is often calculated using the Cramér-Rao lower bound (CRLB), that is, the inverse of the Fisher information.[4,6,7] The latter represents the amount of information the data provides about an unknown parameter.[8,9] The calculation of the CRLB, however, so far relied on an analytical expression for the image of the object, which we refer to as the image function.[6,10] In practice, this can be problematic owing to the fact that often no accurate analytical image function is available.[11,12] Even if an appropriate analytical model is available for the image function, the lack of knowledge about the precise values of imaging parameters might also impose difficulties in the calculation of the CRLB, as analytical image functions are typically functions of the parameters of the imaging setup (see e.g. Torok et al.[13]).

A few approaches are reported in the literature to address the model mismatch issue. For instance, in Liu et al.[14] a phase-retrieved pupil function was used to generate a more accurate model for the point spread function (PSF) of the optical system. This more accurate PSF model was then used for the calculation of the CRLB. In Quirin et al.[15] a similar approach was used to model engineered PSFs. Such techniques, however, are limited to point-like objects and are potentially susceptible to parameter mismatch, since phase retrieval algorithms typically take a variety of imaging parameters, such as the numerical aperture of the objective lens, as inputs.[14]

Send correspondence to Raimund J. Ober, E-mail: raimund.ober@tamu.edu

Nanoimaging and Nanospectroscopy III, edited by Prabhat Verma, Alexander Egner, Proc. of SPIE
Vol. 9554, 955402 · © 2015 SPIE · CCC code: 0277-786X/15/$18 · doi: 10.1117/12.2192008

We have developed a new approach to address the above model and parameter mismatch issues which directly makes use of an experimental image set to calculate the CRLB for a general object.[16] A continuously differentiable representation of the experimental image set is necessary to obtain certain derivatives that are required for the calculation of the CRLB.[4] To achieve such a continuously differentiable model we fit splines, i.e. smoothly connected piecewise polynomials, to the experimentally collected image set.[17] We use splines since they are well-established in image processing and have a number of useful properties. In particular, their derivatives can be obtained analytically.[18] Our proposed method provides the best possible accuracy with which a general subcellular object can be localized without requiring the knowledge of imaging parameters such as the numerical aperture of the objective lens.[16]

Single molecule microscopy is a well-known application of fluorescence microscopy which allows the detection of individual molecules.[1,3] Due to its practical importance, we investigate the application of our approach to single molecule microscopy in more detail. In this case, the object of interest is a single molecule which is typically modeled as a point source[2,4] and, as such, the acquired image set pertains to an experimental PSF. An experimental PSF is a (3D) PSF obtained by (z-stack) imaging a point source, e.g. a bead.[19,20]

We would like to note that in this paper we review some of the results of our recently published journal article[16] and, particularly, apply them for a comparison of the CRLBs of 3D analytical and experimental PSFs.

2. MATERIALS AND METHODS

2.1 Software and Computations

The computations were carried out in a custom-written software package developed in the MATLAB environment (The MathWorks Inc., Natick, MA). This package is capable of calculating the CRLB for 2D and 3D experimental image sets. The computations of the CRLB for analytical PSFs were carried out in the FandPLimitTool,[9,21] which is available online at http://www.wardoberlab.com/software/fandplimittool/.

3. PROBLEM FORMULATION AND THEORY

3.1 Fisher Information Matrix

In this section, we describe the theory for determining the best possible localization accuracy in single molecule microscopy in two and three dimensions. For a 3D localization problem, we denote the location of the object of interest in the object space by the parameter vector $\boldsymbol{\theta} := (x_0, y_0, z_0) \in \Theta$, where $\Theta \subseteq \mathbb{R}^3$, is an open parameter space. For a 2D localization problem, the location parameter vector obviously pertains to $\boldsymbol{\theta} := (x_0, y_0) \in \Theta \subseteq \mathbb{R}^2$. The best possible accuracy with which the location of the object can be estimated, observing its pixelated image, is given by the practical localization accuracy measure (PLAM).[1,4,9] The PLAM is determined using the CRLB.[4,6] According to the Cramér-Rao inequality,[7,8] the covariance matrix of any unbiased estimator $\hat{\boldsymbol{\theta}}$ of a parameter vector $\boldsymbol{\theta} \in \Theta$ is bounded from below by the inverse Fisher information matrix (FIM), i.e. $\mathrm{cov}(\hat{\boldsymbol{\theta}}) \geq \boldsymbol{I}^{-1}(\boldsymbol{\theta})$. The main diagonal elements of the inverse FIM provide lower bounds on the variance of the estimates of the unknown parameters, while we are interested in the estimation accuracy in terms of the standard deviation. Therefore, the PLAM vector is defined as the element-wise square root of the main diagonal entries of the inverse FIM.[9,21]

We next express the FIM for the single molecule microscopy problem. Let $\{C_1, \ldots, C_{K_{\mathrm{pix}}}\}$ be a pixelated detector, where $C_k \subseteq \mathbb{R}^2$ denotes the area occupied by the k^{th} pixel and K_{pix} is the total number of pixels. The pixels are assumed to be disjoint. It has previously been shown that the photon counts detected by the pixels of the detector due to the object of interest are the realizations of independent Poisson random variables with expected values[4,8]

$$\mu_\theta(k) = \frac{N}{M^2} \int_{C_k} q_{z_0}\left(\frac{x}{M} - x_0, \frac{y}{M} - y_0\right) d\boldsymbol{r}, \qquad k = 1, \ldots, K_{\mathrm{pix}}, \tag{1}$$

where $\boldsymbol{r} := (x, y) \in \mathbb{R}^2$, N is the expected number of detected photons on the infinite detector plane (i.e. $\mathbb{R}^2$) due to the object, M is the lateral magnification of the objective lens and q_{z_0} is the image function.[4,6,10] The image function is a bivariate probability density function that describes the image of a stationary object on the detector plane at unit lateral magnification when it is located on the optical axis at position $z_0 \in \mathbb{R}$.[1,6] The

image function for a 2D localization problem is simply given by setting $z_0 = 0$. Interestingly, if the object of interest is a point source, the image function is identical to the PSF of the optical system.[16]

It has been shown that in the presence of extraneous noise, the expression of the FIM is given by[4,6,7]

$$\boldsymbol{I}(\boldsymbol{\theta}) = \sum_{k=1}^{K_{\text{pix}}} \frac{\alpha(k)}{v_\theta(k)} \left(\frac{\partial \mu_\theta(k)}{\partial \boldsymbol{\theta}} \right)^T \frac{\partial \mu_\theta(k)}{\partial \boldsymbol{\theta}}, \qquad \boldsymbol{\theta} \in \Theta, \tag{2}$$

where $v_\theta(k) := \mu_\theta(k) + b_k$ with $b_k,\ k = 1, \ldots, K_{\text{pix}}$, denoting the photon count due to the background signal at pixel C_k. The term $\alpha(k),\ k = 1, \ldots, K_{\text{pix}}$, is the so-called noise coefficient that depends on the extraneous noise sources and the detector type. In the absence of readout noise, $\alpha(k) = 1$ for all $k = 1, \ldots, K_{\text{pix}}$.[4] In the presence of readout noise, the noise coefficient is given by[6,16]

$$\alpha(k) := v_\theta(k) \left(\frac{e^{-v_\theta(k)}}{\sqrt{2\pi}\sigma_k} \int_{\mathbb{R}} \frac{\left(\sum_{l=1}^{\infty} \frac{v_\theta^{l-1}(k)}{(l-1)!} e^{\frac{-(z-l-\eta_k)^2}{2\sigma_k^2}} \right)^2}{\sum_{l=0}^{\infty} \frac{v_\theta^{l}(k)}{l!} e^{\frac{-(z-l-\eta_k)^2}{2\sigma_k^2}}} dz - 1 \right), \qquad k = 1, \ldots, K_{\text{pix}},$$

where η_k and σ_k^2 denote the mean and the variance of the readout noise at pixel C_k, respectively. The expression of the noise coefficient in the presence of readout noise and stochastic signal amplification, i.e. when using an electron multiplying charge-coupled device (EMCCD) camera, can be found in Chao et al.[22]

Supposing that the object of interest is a point source and that an analytical expression is available for the PSF (e.g. the Born and Wolf model[11]), Eq. (2) can be used to calculate the PLAM for a single molecule microscopy experiment. However, as mentioned earlier, the lack of appropriate analytical models for PSFs and the lack of knowledge about the precise values of imaging parameters often pose major challenges in the calculation of the PLAM. To overcome these problems, we have developed an alternative approach by directly making use of an experimental image set for the calculation of the PLAM.[16]

3.2 Experimental Image Sets

A 3D experimental image set is a set of pixelated images of an object acquired at different defocus levels,[20] which are corrupted by extraneous noise during the measurement process.[1,4] Additionally, due to the stochastic nature of light, the acquired images are inherently stochastic.[6,8] Let $z_p \in \mathbb{R},\ p = 1, \ldots, K_{\text{stk}}$, denote the defocus level in the object space, where K_{stk} is the total number of levels. We define an acquired 3D experimental image set as a realization $\{h_{k,p} \in \mathbb{R} \mid k = 1, \ldots, K_{\text{pix}},\ p = 1, \ldots, K_{\text{stk}}\}$ of an array of independent random variables $\{\mathcal{H}_{k,p} \mid k = 1, \ldots, K_{\text{pix}},\ p = 1, \ldots, K_{\text{stk}}\}$ distributed as

$$\mathcal{H}_{k,p} \sim Poisson \left(\frac{N^c}{M^2} \int_{C_k} q_{z_0 - z_p} \left(\frac{x}{M} - x_0, \frac{y}{M} - y_0 \right) dxdy + b_{k,p}^c \right) * \mathcal{N}(0, \sigma_k^{2,c}), \tag{3}$$

where $N^c > 0$ is the expected photon count, $*$ denotes the convolution operator, $b_{k,p}^c \geq 0$ is the background level at pixel $C_k,\ k = 1, \ldots, K_{\text{pix}}$, at defocus level $z_p,\ p = 1, \ldots, K_{\text{stk}}$, and $\mathcal{N}(0, \sigma_k^{2,c})$ denotes a zero-mean Gaussian distribution with variance $\sigma_k^{2,c}$ associated with the readout noise. The above notation can also be used for a 2D localization problem simply by assuming $K_{\text{stk}} = 1$ and $z_p = z_0$. If the object of interest is a point source, the experimental image set pertains to an experimental PSF which can be collected by imaging a bead sample (see e.g. Tahmasbi et al.[16]).

3.3 Spline Fitting

Splines are piecewise polynomials with pieces that are smoothly connected together.[17] One of the important characteristics of a spline is that it can be represented in the form of a linear combination of basis functions known as B-splines. B-splines have a number of important properties, such as affine invariance, local support and positivity,[18] which make them of interest for our application. We therefore take advantage of splines to

estimate the image function. Denote by $\Delta x > 0$, and $\Delta y > 0$, the physical pixel size in the image space in the x and y directions, respectively. Let $\Delta x_0 := \Delta x/M$, and $\Delta y_0 := \Delta y/M$, be the effective pixel size in the object space in the x and y directions, respectively, where M is the lateral magnification of the microscope optics. Let $\Delta z_0 > 0$ be the step size in the z-direction in the object space. A volume spline of degree $d \in \mathbb{N}_0$ with element spacing $(\Delta x_0, \Delta y_0, \Delta z_0)$ in the object space is given by[16]

$$s_a^d(x,y,z) := \sum_{m=1}^{K_{\text{row}}} \sum_{n=1}^{K_{\text{col}}} \sum_{p=1}^{K_{\text{stk}}} a_{m,n,p} \beta^d \left(\frac{x}{\Delta x_0} - n \right) \beta^d \left(\frac{y}{\Delta y_0} - m \right) \beta^d \left(\frac{z}{\Delta z_0} - p \right), \qquad (x,y,z) \in \mathbb{R}^3, \quad (4)$$

where $\{a_{m,n,p} \mid m = 1, \ldots, K_{\text{row}},\ n = 1, \ldots, K_{\text{col}},\ p = 1, \ldots, K_{\text{stk}}\}$ are the B-spline coefficients, K_{row} and K_{col} denote the number of rows and columns of the image, respectively, such that $K_{\text{row}} \times K_{\text{col}} = K_{\text{pix}}$, K_{stk} denotes the total number of defocus levels, and β^d denotes the symmetrical B-spline of degree d given by

$$\beta^d(x) := \sum_{i=0}^{d+1} \frac{(-1)^i}{d!} \binom{d+1}{i} \left(x + \frac{d+1}{2} - i \right)^d u\left(x + \frac{d+1}{2} - i \right), \qquad x \in \mathbb{R}, \quad (5)$$

$$u(x) = \begin{cases} 1, & x \geq 0 \\ 0, & x < 0 \end{cases}.$$

Given the noisy measurements $h_{k,p}$ at pixels $C_k,\ k = 1, \ldots, K_{\text{pix}}$, and at defocus levels $z_p,\ p = 1, \ldots, K_{\text{stk}}$, our problem is to find a volume spline $s_a^d(x,y,z)$ for $(x,y,z) \in \mathbb{R}^3$, such that

$$\int_{C_k} s_a^d \left(\frac{x}{M} - x_0, \frac{y}{M} - y_0, z_p - z_0 \right) dxdy \approx h_{k,p} - b_{k,p}^c, \qquad k = 1, \ldots, K_{\text{pix}},\ p = 1, \ldots, K_{\text{stk}}, \quad (6)$$

where $b_{k,p}^c$ denotes the background level at pixel C_k and at defocus level z_p, and is assumed to be known or can be estimated.[4,16] To introduce a concise matrix notation for the above optimization problem we define

$$\boldsymbol{h} := (h_{1,1} - b_{1,1}^c, \ldots, h_{K_{\text{pix}},1} - b_{K_{\text{pix}},1}^c, h_{1,2} - b_{1,2}^c, \ldots, h_{K_{\text{pix}},K_{\text{stk}}} - b_{K_{\text{pix}},K_{\text{stk}}}^c)^T \in \mathbb{R}^K,$$

$$\boldsymbol{a} := (a_{1,1,1}, \ldots, a_{K_{\text{row}},1,1}, a_{1,2,1}, \ldots, a_{K_{\text{row}},K_{\text{col}},1}, a_{1,1,2}, \ldots, a_{K_{\text{row}},K_{\text{col}},K_{\text{stk}}})^T \in \mathbb{R}^K,$$

where $K := K_{\text{pix}} \times K_{\text{stk}}$ is the total number of data points. We also define $\boldsymbol{S} \in \mathbb{R}^{K \times K}$ such that for $k = 1, \ldots, K_{\text{pix}},\ i, p = 1, \ldots, K_{\text{stk}},\ m = 1, \ldots, K_{\text{row}}$, and $n = 1, \ldots, K_{\text{col}}$

$$\boldsymbol{S}_{k+(i-1)K_{\text{pix}},m+(n-1)K_{\text{row}}+(p-1)K_{\text{pix}}} = \int_{C_k} \beta^d \left(\frac{\frac{x}{M} - x_0}{\Delta x_0} - n \right) \beta^d \left(\frac{\frac{y}{M} - y_0}{\Delta y_0} - m \right) d\boldsymbol{r} \beta^d \left(\frac{z_i - z_0}{\Delta z_0} - p \right),$$

where $\boldsymbol{r} = (x,y) \in \mathbb{R}^2$. We now define $\boldsymbol{B} \in \mathbb{R}^{K \times K}$ such that for $m, m' = 1, \ldots, K_{\text{row}},\ n, n' = 1, \ldots, K_{\text{col}},\ p, p' = 1, \ldots, K_{\text{stk}}$,

$$\boldsymbol{B}_{(p-1)K_{\text{pix}}+(n-1)K_{\text{row}}+m,(p'-1)K_{\text{pix}}+(n'-1)K_{\text{row}}+m'} = \sum_{q_1+q_2+q_3=l} \binom{l}{q_1, q_2, q_3} B_{\Delta x_0}^{q_1}(n,n') B_{\Delta y_0}^{q_2}(m,m') B_{\Delta z_0}^{q_3}(p,p'),$$

where

$$B_\Delta^q(n,n') := \int_{\mathbb{R}} \frac{\partial^q}{\partial t^q} \beta^d \left(\frac{t}{\Delta} - n \right) \frac{\partial^q}{\partial t^q} \beta^d \left(\frac{t}{\Delta} - n' \right) dt, \qquad n, n' \in \mathbb{N},\ q = 1, \ldots, l,\ \Delta > 0.$$

To estimate the B-spline coefficients in the presence of stochasticity and noise, by making use of the matrix notation introduced above, we solve the following optimization problem (for more details see[16])

$$\hat{\boldsymbol{a}} = \underset{\boldsymbol{a} \in \mathbb{R}^K}{\operatorname{argmin}} \left(\|\boldsymbol{h} - \boldsymbol{S}\boldsymbol{a}\|^2 + \gamma \boldsymbol{a}^T \boldsymbol{B} \boldsymbol{a} \right), \quad (7)$$

which is a regularized least-squares problem.[17,18] The first term measures the error between the data and the model in the least squares sense and the second term imposes a smoothness constraint on the solution. The regularization (smoothing) factor $\gamma \geq 0$ controls the trade-off between fidelity to the data and the smoothness of the estimate. Using vector differentiation,[16] it is easy to verify that the minimizer to Eq. (7) is given by the solution of the following equation

$$\left(\boldsymbol{S}^T\boldsymbol{S} + \gamma\boldsymbol{B}\right)\hat{\boldsymbol{a}} = \boldsymbol{S}^T\boldsymbol{h}, \tag{8}$$

which can be solved efficiently using Gaussian elimination. We would like to note that the solution of the above equation can be obtained given a specific choice of the smoothing factor γ, the derivative order l and the B-spline degree d. The smoothing factor can be chosen based on a priori information, e.g. the variance of the measurement noise. The typical choice for the derivative order in modern statistics literature is $l = 2$, although other orders can also be easily used.[16] Given the order of derivatives, an appropriate degree for the B-splines can be chosen as $d = 2l - 1$.[18]

3.4 Calculation of the Fisher Information Matrix

After estimating the B-spline coefficients $\hat{\boldsymbol{a}}$ using Eq. (8), one can substitute them into Eq. (4) and obtain the spline fit to the experimental image set $\boldsymbol{h}$. This volume fit $\hat{s}_a^d$ after normalization can be used to obtain an estimate of the image function. For conciseness, define $\sum_{m,n,p} := \sum_{m=1}^{K_{\text{row}}}\sum_{n=1}^{K_{\text{col}}}\sum_{p=1}^{K_{\text{stk}}}$. The normalization factor is defined as (see Tahmasbi et al.[16] for details)

$$C(z_0) := \Delta x_0 \Delta y_0 \sum_{m,n,p} \hat{a}_{m,n,p}\beta^d\left(\frac{z_0}{\Delta z_0} - p\right), \qquad z_0 \in \mathbb{R}. \tag{9}$$

The estimated image function is given by

$$\hat{q}_{z_0}(x,y) := \frac{\hat{s}_a^d(x,y,z_0)}{C(z_0)} = \sum_{m,n,p} \tilde{a}_{m,n,p}^{z_0}\beta^d\left(\frac{x}{\Delta x_0} - n\right)\beta^d\left(\frac{y}{\Delta y_0} - m\right)\beta^d\left(\frac{z_0}{\Delta z_0} - p\right),$$

where $(x,y) \in \mathbb{R}^2$, and $\tilde{a}_{m,n,p}^{z_0} := \hat{a}_{m,n,p}/C(z_0),\ m = 1,\ldots,K_{\text{row}},\ n = 1,\ldots,K_{\text{col}},\ p = 1,\ldots,K_{\text{stk}}$, are termed the normalized B-spline coefficients.

We now have an estimate of the image function that can be used to calculate the PLAM. Substituting the estimated image function into Eq. (1), for $k = 1,\ldots,K_{\text{pix}}$, we have

$$\mu_\theta(k) \approx \frac{N}{M^2}\sum_{m,n,p}\tilde{a}_{m,n,p}^{z_0}\int_{C_k}\beta^d\left(\frac{\frac{x}{M} - x_0}{\Delta x_0} - n\right)\beta^d\left(\frac{\frac{y}{M} - y_0}{\Delta y_0} - m\right)d\boldsymbol{r}\beta^d\left(\frac{z_0}{\Delta z_0} - p\right). \tag{10}$$

An important property of B-spline functions is that their first derivatives can be obtained analytically using the following expression[16,17]

$$\frac{\partial\beta^d(x)}{\partial x} = \beta^{d-1}(x + \frac{1}{2}) - \beta^{d-1}(x - \frac{1}{2}), \qquad x \in \mathbb{R},\ d \in \mathbb{N}. \tag{11}$$

Using this identity and taking the partial derivatives of both sides of Eq. (10) with respect to x_0 for $k = 1,\ldots,K_{\text{pix}}$, we have (for details see[16])

$$\begin{aligned}\frac{\partial\mu_\theta(k)}{\partial x_0} \approx \frac{-N}{M^2}\sum_{m=1}^{K_{\text{row}}}\sum_{n=1}^{K_{\text{col}}+1}\sum_{p=1}^{K_{\text{stk}}}\frac{\tilde{a}_{m,n,p}^{z_0} - \tilde{a}_{m,n-1,p}^{z_0}}{\Delta x_0}\beta^d\left(\frac{z_0}{\Delta z_0} - p\right)\\ \times\int_{C_k}\beta^{d-1}\left(\frac{\frac{x}{M} - x_0}{\Delta x_0} - n + \frac{1}{2}\right)\beta^d\left(\frac{\frac{y}{M} - y_0}{\Delta y_0} - m\right)d\boldsymbol{r},\end{aligned}$$

where $\boldsymbol{r} = (x, y) \in \mathbb{R}^2$ and we assumed $\tilde{a}^{z_0}_{m,0,p} = \tilde{a}^{z_0}_{m,K_{\rm col}+1,p} = 0$, $m = 1, \ldots, K_{\rm row}$, $p = 1, \ldots, K_{\rm stk}$. Similarly, we can obtain the partial derivatives with respect to y_0 for $k = 1, \ldots, K_{\rm pix}$, as follows

$$\frac{\partial \mu_\theta(k)}{\partial y_0} \approx \frac{-N}{M^2} \sum_{m=1}^{K_{\rm row}+1} \sum_{n=1}^{K_{\rm col}} \sum_{p=1}^{K_{\rm stk}} \frac{\tilde{a}^{z_0}_{m,n,p} - \tilde{a}^{z_0}_{m-1,n,p}}{\Delta y_0} \beta^d \left(\frac{z_0}{\Delta z_0} - p \right) \times \int_{C_k} \beta^d \left(\frac{\frac{x}{M} - x_0}{\Delta x_0} - n \right) \beta^{d-1} \left(\frac{\frac{y}{M} - y_0}{\Delta y_0} - m + \frac{1}{2} \right) d\boldsymbol{r},$$

where $\tilde{a}^{z_0}_{0,n,p} = \tilde{a}^{z_0}_{K_{\rm row}+1,n,p} = 0$, for all $n = 1, \ldots, K_{\rm col}$, and $p = 1, \ldots, K_{\rm stk}$. We can also derive the partial derivatives with respect to z_0 for $k = 1, \ldots, K_{\rm pix}$, as follows (see[16] for details)

$$\frac{\partial \mu_\theta(k)}{\partial z_0} \approx \frac{N}{M^2} \sum_{m=1}^{K_{\rm row}} \sum_{n=1}^{K_{\rm col}} \sum_{p=1}^{K_{\rm stk}+1} \frac{\tilde{a}^{z_0}_{m,n,p} - \tilde{a}^{z_0}_{m,n,p-1}}{\Delta z_0} \beta^{d-1} \left(\frac{z_0}{\Delta z_0} - p + \frac{1}{2} \right) \times \int_{C_k} \beta^d \left(\frac{\frac{x}{M} - x_0}{\Delta x_0} - n \right) \beta^d \left(\frac{\frac{y}{M} - y_0}{\Delta y_0} - m \right) d\boldsymbol{r} - \mu_\theta(k) \xi(z_0), \tag{12}$$

where $\tilde{a}^{z_0}_{m,n,0} = \tilde{a}^{z_0}_{m,n,K_{\rm stk}+1} = 0$, for all $m = 1, \ldots, K_{\rm row}$, and $n = 1, \ldots, K_{\rm col}$, and for $z_0 \in \mathbb{R}$,

$$\xi(z_0) := \frac{1}{C(z_0)} \frac{\partial C(z_0)}{\partial z_0} = \frac{\Delta x_0 \Delta y_0}{\Delta z_0} \sum_{m=1}^{K_{\rm row}} \sum_{n=1}^{K_{\rm col}} \sum_{p=1}^{K_{\rm stk}+1} (\tilde{a}^{z_0}_{m,n,p} - \tilde{a}^{z_0}_{m,n,p-1}) \beta^{d-1} \left(\frac{z_0}{\Delta z_0} - p + \frac{1}{2} \right).$$

4. RESULTS

4.1 Experimental PSF Example

We have developed an approach for the calculation of the best possible accuracy with which a general object can be localized, i.e. the PLAM, directly from 2D and 3D experimental image sets. Here we primarily focus on point-like objects (e.g. a single molecule) and, as such, the experimental image set pertains to an experimental PSF. We refer to the PLAM deduced from an experimental PSF using the aforementioned approach as the experimental PLAM, whereas the PLAM calculated from an analytical PSF is referred to as the analytical PLAM. We further refer to the limit of the localization accuracy for the x, y and z coordinates of the single molecule as x_0-PLAM, y_0-PLAM and z_0-PLAM, respectively.

We now provide an example to investigate the performance of the proposed approach in practice and compare the results with those for an analytical PSF model. In particular, we use the collected 3D experimental PSF of a microscopy setup which was reported in Section 2.1 of Tahmasbi et al.[16] We have deliberately used a setup with an aberrated PSF as it is a good example to illustrate the practical performance of the proposed approach. Figures 1(a) and 1(b) show the yz- and xy-projections of the acquired experimental PSF, respectively. To suppress the stochasticity and noise in the collected experimental PSF, based on the analyses reported in,[16] we fit a volume smoothing spline of appropriate degree and smoothing factor to the experimental PSF. The yz- and xy-projections of the smoothing spline fit are shown in Figs. 1(a') and 1(b'), respectively, where we see a marked suppression of the extraneous noise.

Figures 1(c) and 1(d) show the experimental x_0-PLAM and z_0-PLAM, respectively, along the z-axis which are taken from Tahmasbi et al.[16] (the experimental y_0-PLAM is analogous to x_0-PLAM and is not shown). For comparison purposes, we calculated the analytical PLAM assuming the Born and Wolf 3D PSF model with a set of imaging parameters which are similar to those used for the collection of the experimental PSF. The analytical x_0-PLAM and z_0-PLAM along the z-axis are also shown in Figs. 1(c) and 1(d), respectively. The experimental x_0-PLAM has smaller numerical values at or close to the plane of focus and increases as the particle moves away. This is an expected result for typical 3D PSFs and is similar to the behavior of the x_0-PLAM for the Born and Wolf PSF (see Fig. 1(c)).[1] An important observation is that the experimental x_0-PLAM is consistently larger than the analytical x_0-PLAM along the z-axis. This is to a large degree due to the mismatch between the

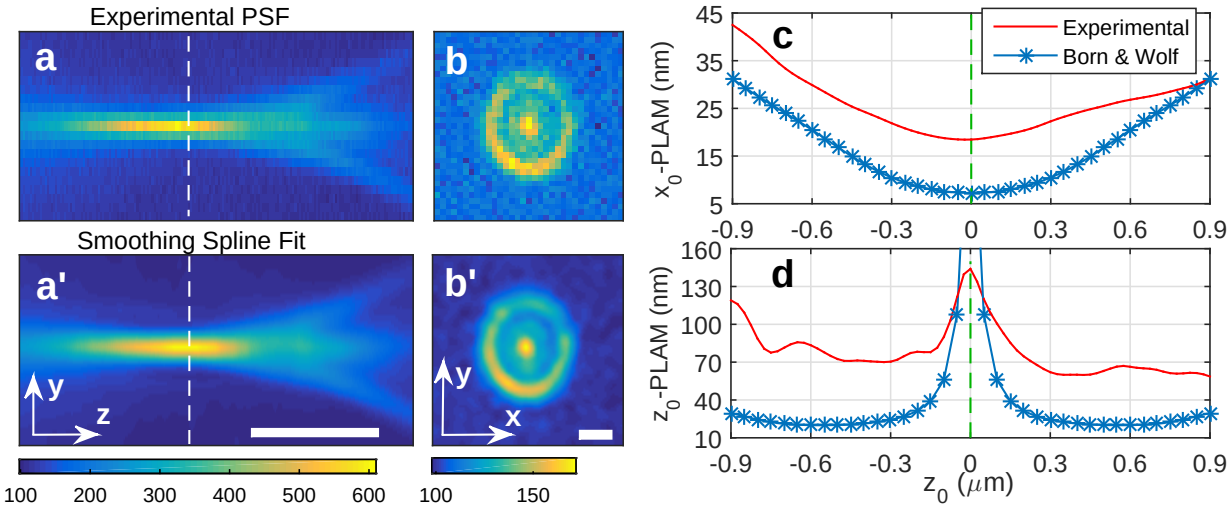

Figure 1. Comparison of the PLAM for an experimental PSF with that of the Born and Wolf model. (a), (b) The yz-projection and the xy-projection (at $z_0 = 2.6$ μm) of a deliberately aberrated experimentally collected PSF from a practical microscopy setup, respectively, where the ROI size is 33×33 pixels (other parameters are reported in Section 2.1 of Tahmasbi et al.[16]). (a'), (b') The corresponding yz- and xy-projections of the cubic volume spline fit with a smoothing factor of $\gamma = 0.01$, which is evaluated on a finer grid (color scale bars are in photons). The vertical dashed lines show the location of the plane of focus and the size bars are 1.5 μm (panels (a) and (a') are stretched in the z-direction for better visualization). The estimated photon count and background level of the bead sample are approximately $N^c = 4500$ photons and $b^c = 16$ photons/pixel, respectively. (c), (d) The experimental x_0-PLAM and z_0-PLAM, respectively, along the z-axis (the reported results are the average of the results for multiple beads) overlaid with analytical x_0-PLAM and z_0-PLAM calculated using the Born and Wolf PSF model simulated considering similar imaging parameters. For the calculation of the PLAMs we assumed $N = 500$ photons and $b = 10$ photons/pixel.

nominal values for imaging parameters, such as the numerical aperture of the objective and the refractive index of the immersion oil, and their achievable values in practice. A subtle point in the behavior of the experimental x_0-PLAM is that it is not symmetric with respect to the plane of focus. For example, the numerical value of the x_0-PLAM is 30 nm at $z_0 = -0.6$ μm, whereas it is approximately 26 nm at $z_0 = 0.6$ μm. This is not surprising since any mismatch between the refractive indices of the sample and immersion medium contributes to an axially asymmetric PSF.[12]

Additionally, the experimental z_0-PLAM is large near or at the focal plane, e.g. it is 144 nm at the focal plane, and decreases as the point source moves away from the focal plane (see Fig. 1(d)). The large numerical value of the experimental z_0-PLAM at the focal plane is often referred to as the depth discrimination problem and is expected (see e.g.[9]). However, note that the numerical value of the experimental z_0-PLAM at the focal plane is still considerably smaller than that of the analytical z_0-PLAM for the Born and Wolf PSF model, which tends to infinity. This behavior of the experimental z_0-PLAM can be explained by the axial asymmetry of the experimental PSF caused by the mismatch between the refractive indices of the sample and immersion oil.[12] By contrast, the Born and Wolf PSF model is perfectly axially symmetric and therefore does not provide any information about the z_0-location of a single molecule when it is at the plane of focus. Finally, the considerable difference between the numerical values of the experimental and analytical z_0-PLAMs at larger z-positions is to a large extent due to the mismatch between the nominal values of the imaging parameters and their practical values.

ACKNOWLEDGMENTS

This work was supported in part by the National Institutes of Health (R01 GM085575).

REFERENCES

1. Ober, R. J., Tahmasbi, A., Ram, S., Lin, Z., and Ward, E. S., "Quantitative aspects of single molecule microscopy: Information-theoretic analysis of single-molecule data," *IEEE Signal Process. Mag.* **32**, 58–69 (2015).
2. Deschout, H., Zanacchi, F. C., Mlodzianoski, M., Diaspro, A., Bewersdorf, J., Hess, S. T., and Braeckmans, K., "Precisely and accurately localizing single emitters in fluorescence microscopy," *Nat. Methods* **11**, 253–266 (2014).
3. Small, A. and Stahlheber, S., "Fluorophore localization algorithms for super-resolution microscopy," *Nat. Methods* **11**, 267–279 (2014).
4. Ober, R. J., Ram, S., and Ward, E. S., "Localization accuracy in single-molecule microscopy," *Biophys. J.* **86**, 1185–1200 (2004).
5. Betzig, E., Patterson, G. H., Sougrat, R., Lindwasser, O. W., Olenych, S., Bonifacino, J. S., Davidson, M. W., Lippincott-Schwartz, J., and Hess, H. F., "Imaging intracellular fluorescent proteins at nanometer resolution," *Science* **313**, 1642–1645 (2006).
6. Ram, S., Ward, E. S., and Ober, R. J., "A stochastic analysis of performance limits for optical microscopes," *Multidim. Sys. Sig. Proc.* **17**, 27–57 (2006).
7. Ram, S., Ward, E. S., and Ober, R. J., "A stochastic analysis of distance estimation approaches in single molecule microscopy: quantifying the resolution limits of photon-limited imaging systems," *Multidim. Sys. Sig. Proc.* **24**, 503–542 (2013).
8. Snyder, D. L. and Miller, M. I., [*Random Point Processes in Time and Space*], Springer Verlag, New York, USA, second ed. (1991).
9. Tahmasbi, A., Ram, S., Chao, J., Abraham, A. V., Tang, F. W., Ward, E. S., and Ober, R. J., "Designing the focal plane spacing for multifocal plane microscopy," *Opt. Express* **22**, 16706–16721 (2014).
10. Tahmasbi, A., Ram, S., Chao, J., Abraham, A. V., Ward, E. S., and Ober, R. J., "An information-theoretic approach to designing the plane spacing for multifocal plane microscopy," *Proc. SPIE* **9330**, 933011 (2015).
11. Born, M. and Wolf, E., [*Principles of Optics*], Cambridge University Press, Cambridge, UK, seventh ed. (2002).
12. Gibson, S. F. and Lanni, F., "Experimental test of an analytical model of aberration in an oil-immersion objective lens used in three-dimensional light microscopy," *J. Opt. Soc. Am. A* **9**, 154–166 (1992).
13. Torok, P. and Kao, F. J., [*Optical Imaging and Microscopy*], Springer Verlag, New York, USA, first ed. (2003).
14. Liu, S., Kromann, E., Krueger, W., Bewersdorf, J., and Lidke, K., "Three dimensional single molecule localization using a phase retrieved pupil function," *Opt. Express* **21**, 29462–29487 (2013).
15. Quirin, S., Pavani, S. R. P., and Piestun, R., "Optimal 3d single-molecule localization for superresolution microscopy with aberrations and engineered point spread functions," *Proc. Natl. Acad. Sci. USA* **109**, 675–679 (2012).
16. Tahmasbi, A., Ward, E. S., and Ober, R. J., "Determination of localization accuracy based on experimentally acquired image sets: applications to single molecule microscopy," *Opt. Express* **23**, 7630–7652 (2015).
17. Unser, M., "Splines: a perfect fit for signal and image processing," *IEEE Signal Process. Mag.* **16**, 22–38 (1999).
18. Unser, M., Aldroubi, A., and Eden, M., "B-spline signal processing: part itheory," *IEEE Trans. Signal Process.* **41**, 821–832 (1993).
19. Lai, X., Lin, Z., Ward, E. S., and Ober, R. J., "Noise suppression of point spread functions and its influence on deconvolution of three-dimensional fluorescence microscopy image sets," *J. Microsc.* **217**, 93–108 (2005).
20. Claxton, C. D. and Staunton, R. C., "Measurement of the point-spread function of a noisy imaging system," *J. Opt. Soc. Am. A* **25**, 159–170 (2008).
21. Abraham, A. V., Ram, S., Chao, J., Ward, E. S., and Ober, R. J., "Quantitative study of single molecule location estimation techniques," *Opt. Express* **17**, 23352–23373 (2009).
22. Chao, J., Ward, E. S., and Ober, R. J., "Fisher information matrix for branching processes with application to electron-multiplying charge-coupled devices," *Multidim. Sys. Sig. Proc.* **23**, 349–379 (2012).